

REFINE-BY-ALIGN: REFERENCE-GUIDED ARTIFACTS REFINEMENT THROUGH SEMANTIC ALIGNMENT

Anonymous authors

Paper under double-blind review



Figure 1: *Refine-by-Align*. Given a generated image (with artifacts), a free-form mask indicating the artifacts region in the generated image, and a high-quality reference image containing important details such as identity logo or font, our model can automatically refine the artifacts in the generated image by leveraging the corresponding details from the reference. The proposed method could benefit various applications (e.g., DreamBooth (Ruiz et al., 2023a) for text-to-image customization, IDM-VTON (Choi et al., 2024) for virtual try-on, AnyDoor (Chen et al., 2023) for object composition, and Zero 1-to-3++ (Shi et al., 2023b) for novel view synthesis).

ABSTRACT

Personalized image generation has emerged from the recent advancements in generative models. However, these generated personalized images often suffer from localized artifacts such as incorrect logos, reducing fidelity and fine-grained identity details of the generated results. Furthermore, there is little prior work tackling this problem. To help improve these identity details in the personalized image generation, we introduce a new task: *reference-guided artifacts refinement*. We present **Refine-by-Align**, a first-of-its-kind model that employs a diffusion-based framework to address this challenge. Our model consists of two stages: **Alignment Stage** and **Refinement Stage**, which share weights of a unified neural network model. Given a generated image, a masked artifact region, and a reference image, the alignment stage identifies and extracts the corresponding regional features in the reference, which are then used by the refinement stage to fix the artifacts. Our model-agnostic pipeline requires no test-time tuning or optimization. It automatically enhances image fidelity and reference identity in the generated image, generalizing well to existing models on various tasks including but not limited to customization, generative compositing, view synthesis, and virtual try-on. Extensive experiments and comparisons demonstrate that our pipeline greatly pushes the boundary of fine details in the image synthesis models.

1 INTRODUCTION

Generative models for image synthesis (Ho et al., 2020; Rombach et al., 2022; Peebles & Xie, 2023; Podell et al., 2023; Luo et al., 2023b) have made significant advancement. Moreover, recent diffusion models (DM) enable reference-guided image generation, where a text and/or visual prompt is provided and the subject object is generated in a specified novel context. This ability has been widely applied to applications such as subject customization (Ruiz et al., 2023a), object composition (Chen et al., 2023), novel view synthesis (Shi et al., 2023b) and virtual try-on (Choi et al., 2024). While these works seek generation in a single step, in practice undesired blemishes, detail omissions, and blurriness may occur in the generated images. These localized unpleasant anomalies are typically called *artifacts* as perceived by human eyes (e.g., "artifacts" row in Figure 1 (Zhang et al., 2023b)). The artifacts reduce image fidelity and the overall prompt-alignment quality of the synthesized images. Thus, a localized refinement tool to remove or reduce artifacts is beneficial.

Recently, a few limited approaches to artifact detection and refinement have been presented. PAL (Zhang et al., 2023b) presents an early work in this area that trains an artifact detection model in a supervised end-to-end manner using input images with artifacts and corresponding ground truth images. The detected artifacts can be partially removed using a pre-trained image inpainting tool. As PAL identifies, the artifacts are typically very small and irregular-shaped (Appendix Fig. 8), which further complicates the refinement process. PAL ameliorates artifacts but struggles with diversity of artifact refinement. Lack of diversity is also observed in RealHuman (Wang et al., 2024a) that focuses on artifacts in human hands and faces, and the SynArtifact (Cao et al., 2024) using vision-language model and reinforcement learning for artifact annotation and removal. In general, none of these methods are able to provide a controllable and predictable artifact refinement output with free-form support automatically to precisely preserve the original identity details.

Our main approach is to leverage the identity detail info in the reference-image to guide the refine the artifacts. This provides a locally-controllable output (i.e., we specify the desired refinement), works for arbitrarily-shaped artifacts, preserves the identity and background in the provided generated image, and is applicable to multiple image generation approaches. As shown in Fig. 1, we provide *reference-guided artifacts refinement*: Given a generated image with marked artifact regions, and a reference image (containing a reference object), our model refines the artifacts by transferring corresponding details from the reference image to the artifact regions in the originally generated image. Our reference-guided approach shares insights with many reference-based image customization models (Song et al., 2023; Chen et al., 2023; Yang et al., 2023), but those models overlooked the accurate region-alignment between reference image and artifact region. In Fig. 2, SOTA models specialized on finding correspondences may fail on key point matching for arbitrary-shaped regions.

Our approach proceeds in two stages (Fig. 3). (1) **Alignment Stage**: we design a novel alignment algorithm (Algorithm 1) for arbitrarily-shaped regional feature matching which utilizes the artifact regions to query corresponding features from the reference image. In particular, the best match is obtained by maximizing the spatial correlation between DM-captured cross-attention maps of both

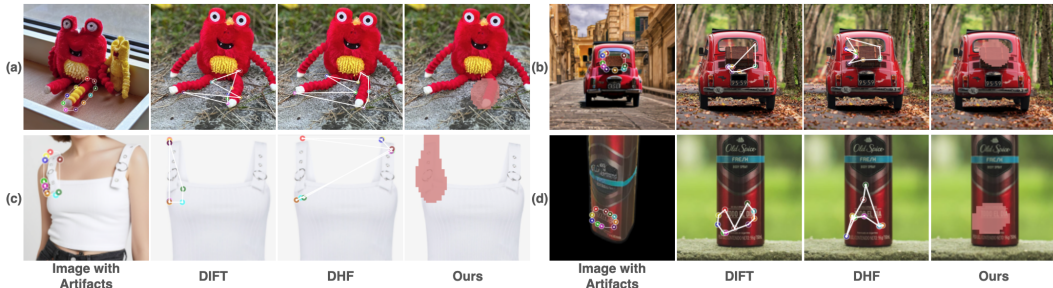


Figure 2: Comparisons of our region-matching method with keypoint matching. We utilize DIFT (Tang et al., 2023) and DHF (Luo et al., 2023a) to perform keypoint matching from the artifacts region (10 points are sampled along the artifacts contour) to the reference. DIFT and DHF often fail to find the accurate corresponding region; in addition, they have trouble in distinguishing between repeating patterns such as (a)(c). In contrast, our method is more robust. The results demonstrate that artifacts alignment is a non-trivial process.

artifact region and the reference image. (2) **Refinement Stage**: we train a diffusion model to use the best matched features from the alignment stage to refine the artifact region and preserve identity. Our model is trained in a self-supervised scheme and we demonstrate its application to artifacts generated by various generative models. Quantitative and qualitative comparisons (i.e., using several well-established metrics and a user study; Sec. 4.2, Sec. 4.3) show that in terms of detail and appearance preservation our model outperforms all six baseline models (Paint-by-Example (Yang et al., 2023), ObjectStitch (Song et al., 2023), AnyDoor (Chen et al., 2023), PAL (Zhang et al., 2023b), Cross-Image Attention (Alaluf et al., 2024) and MimicBrush (Chen et al., 2024)).

Our contributions can be summarized as follows:

- A first-of-its-kind generative artifacts refinement framework supporting control via reference image specification, identity preservation, arbitrary artifact shapes and sizes, and good fidelity.
- A novel artifacts matching algorithm which matches arbitrarily-shaped artifacts to corresponding patterns in the reference image.
- An effective reference-guided refinement strategy that ameliorates artifacts in a provided generated image.
- A comprehensive benchmark, *GenArtifactBench*, consisting of artifacts generated by several well-known models, reference images, and dense human annotations which can serve to evaluate future efforts in this area.

2 RELATED WORK

2.1 REFERENCE-GUIDED IMAGE EDITING

Reference-guided image editing has been a traditional task that has various applications, including reference-guided super resolution (Zhang et al., 2019; Jiang et al., 2022), and guided inpainting or outpainting (Zhou et al., 2021; Tang et al., 2024). With the significant advancements in diffusion models (DM) (Ho et al., 2020; Sohl-Dickstein et al., 2015; Song & Ermon, 2019; Rombach et al., 2022; Ho & Salimans, 2022; Peebles & Xie, 2023) in text-to-image (T2I) synthesis, there have been many works on subject-driven image editing. The notion of using an additional reference image to guide image editing (e.g., (Ruiz et al., 2023a; Kavar et al., 2023)) has led to a series of techniques (Ruiz et al., 2023b; Gal et al., 2022; Shi et al., 2023a; Kumari et al., 2023; Liu et al., 2023b) using optimization to learn concepts. In spite of their high-fidelity editing results, they usually require inference time fine-tuning or multiple subject images. Another branch of works (Yang et al., 2023; Song et al., 2023; Chen et al., 2023; Zhang et al., 2024; Li et al., 2024) replace the text embedding of T2I models with image embedding based on CLIP or DINOv2 (Radford et al., 2021; Oquab et al., 2023; Song et al., 2024), which are tuning-free. Subsequent works have extended the applications to image compositing (Lu et al., 2023; Wang et al., 2024b; Avrahami et al., 2022; Sarukkai et al., 2024; Meng et al., 2021), novel view synthesis (Liu et al., 2023a; Shi et al., 2023b; Liu et al., 2024) and subject swapping (Gu et al., 2023; 2024). However, they all face a critical challenge of controllability and identity preservation of the original object.

2.2 CORRESPONDENCE MATCHING

Traditional methods use carefully-designed features (Bay et al., 2006; Lowe, 2004; Rublee et al., 2011) or learning-based approaches (Aberman et al., 2018; Rocco et al., 2018; Seo et al., 2018; Simonyan et al., 2014) to establish correspondences. Recent work has shifted towards adapting diffusion models. Tang et al. (2023); Luo et al. (2023a); Zhang et al. (2023a); Hedlin et al. (2023) leverage the features maps or embeddings of pretrained DMs to predict correspondences. Appearance transfer (Go et al., 2024; Chen et al., 2024; Alaluf et al., 2024) is a downstream application of such task. However, they still suffer from the loss of fine-grained identity details from the reference.

2.3 LOCALIZATION AND REFINEMENT OF ARTIFACTS

It is challenging for the state-of-the-art models to capture intricate details, such as object textures and human hands. In Zhang et al. (2023b), these artifacts are defined as *implausible content or*

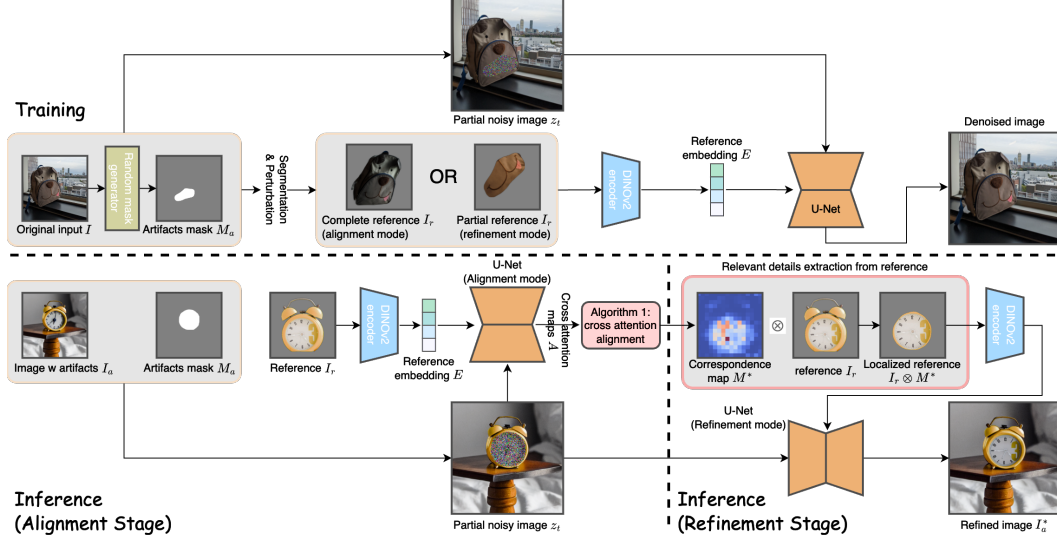


Figure 3: **Overview of our framework.** *Top:* During training, we train a DM for object completion, guided by a reference image I_r . In alignment mode, the reference is a complete object, so the model learns to locate the relevant region from the reference for object completion, thus maximizing the spatial correlation in attention maps. In refinement mode, this region is directly provided as reference. *Bottom:* During inference, the inputs include a generated image I_a with the artifacts marked as M_a , and a reference object I_r . In the alignment stage, we perform **cross-attention alignment** algorithm (see Alg. 1 and Fig. 5) to find the correspondence map M^* . In the refinement stage, M^* is used to find the region in I_r that corresponds to artifacts, which guides refining to I_a .

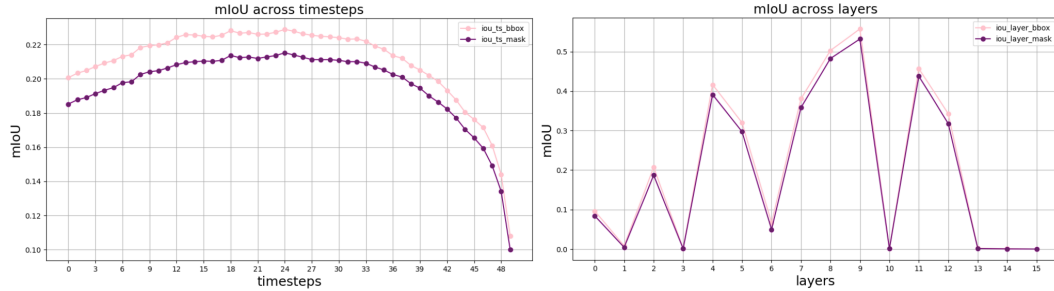


Figure 4: Running the cross-attention alignment algorithm on GenArtifactBench to find the best combination of timestep t and transformer layer l . *Left:* mIoU across all timesteps, averaged over all layers and images; *Right:* mIoU across all layers, averaged over all timesteps and images.

display of unpleasant artifacts in specific regions of the image. Although artifacts are commonly observed even in the leading generative models, few works have explored the topic of artifacts detection and refinement. Recently, Zhang et al. (2023b) curate a human-annotated dataset for artifact segmentation, train a segmentation model for artifact localization and a zoom-in inpainting pipeline for refinement. Cao et al. (2024) classify the artifacts and fine-tune T2I DMs to reduce artifacts. Specifically in handling artifacts on human body, Wang et al. (2024a) propose an approach to refine artifacts in faces and hands. Concurrently, Chen et al. (2024) propose MimicBrush for appearance transfer, which is a potential use for artifact refinement. However, none of these works are designed to perform reference-guided artifacts refinement, thus lacks control. For the first time, we provide a solution for guided artifacts refinement with fine-grained control.

3 METHOD

The proposed artifacts refinement framework, Refine-by-Align, is shown in Fig. 3. Formally, we define the task of artifacts refinement conditioned on a reference image as following: Let $I_a \in \mathbb{R}^{H \times W \times 3}$ be an image with artifacts generated by any reference-guided generation model, $M_a \in \mathbb{R}^{H \times W}$ be a user provided artifacts mask, $I_r \in \mathbb{R}^{H \times W \times 3}$ be the segmented reference object image;

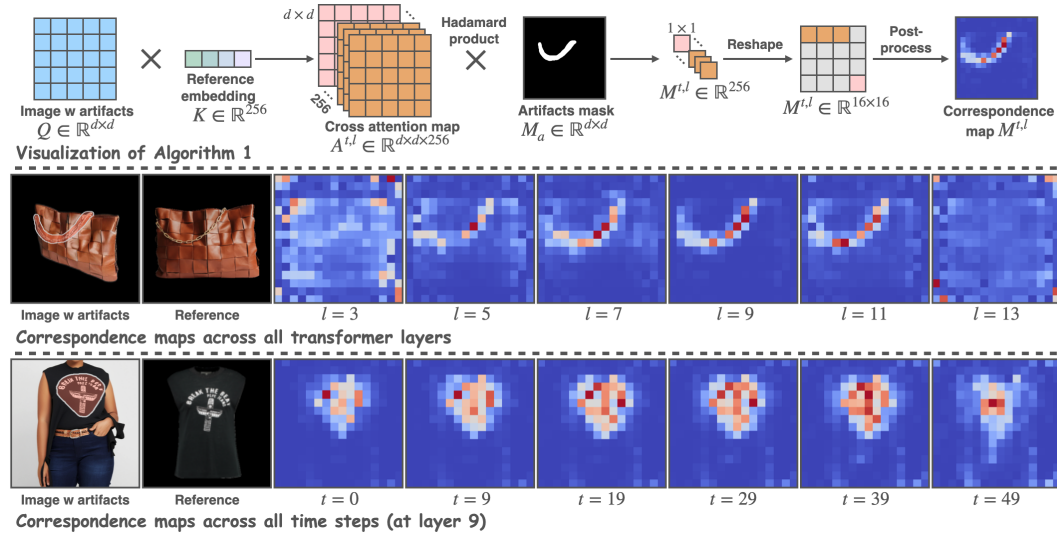


Figure 5: *Top*: Visualization of our cross-attention alignment algorithm. The artifacts mask is used to extract the spatial correlations between the artifacts and the reference; the output of this algorithm, the correspondence map, indicates the region in the reference that corresponds to the artifacts area. *Middle and Bottom*: Correspondence maps across different transformer layers and timesteps.

Algorithm 1 Optimal Cross-Attention Alignment (refer to Fig. 5 for visualization)

Input: Target image I , resized artifacts mask $M_a \in \mathbb{R}^{d \times d}$, reference image I_r , DINOv2 encoder ϕ , the refinement model \mathcal{R} , the ground truth correspondence mask M_{gt} on I_r .

Parameter: The diffusion time steps T , total number of transformer block L in \mathcal{R} , the noisy image resolution d in latent space.

Output: Optimal correspondence mask M^* (for I_r).

```

1:  $E \leftarrow \text{MLP}(\phi(I_r)); E \in \mathbb{R}^{256 \times 768}$  ..... # Get reference embedding
2:  $z_T \sim \mathcal{N}(0, I)$ 
3: Zero array  $\Gamma \in \mathbb{R}^{T \times L}$ 
4: for  $t = T - 1, \dots, 0$  do
5:   for  $l = 0, \dots, L - 1$  do
6:      $A^{t,l} \leftarrow \mathcal{R}(z_t, t, E); A^{t,l} \in \mathbb{R}^{(d \times d) \times 256}$  ..... # Extract cross-attention map at  $l$ -th block
7:      $M^{t,l} = \sum_{i,j} (M_a \circ A^{t,l}[i, j, :])$  ..... # 2D correspondence mask on  $I_r$ 
8:      $\Gamma_{t,l} \leftarrow \text{mIoU}(M^{t,l}, M_{gt})$  ..... # Calculate mIoU
9:   end for
10: end for
11:  $t^*, l^* \leftarrow \arg \max_{t,l} (\Gamma)$  ..... # Find optimal  $t$  and  $l$ 
12: return  $M^* \leftarrow M^{t^*, l^*}$ 

```

we train a Diffusion Model (DM)-based refinement model \mathcal{R} to generate a refined image I_a^* :

$$I_a^* = \mathcal{R}(I_a, M_a, I_r) \in \mathbb{R}^{H \times W \times 3} \quad (1)$$

Ideally in I_a^* , the refined area $I_a^* \otimes M_a$ should be consistent with the background and preserve the identity from the reference object I_r ; the whole image I_a^* should appear natural and artifacts-free.

However, directly using I_r as the visual guidance may cause significant degradation. Hence, an **optimal correspondence mask** M^* is necessary for an optimized input reference as $I_r \otimes M^*$ for better guidance. To tackle this task, we created a two stage approach \mathcal{R} : the **Alignment Stage** and the **Refinement Stage**, which share the weights of a single unified neural network model. In the alignment stage, the artifacts region $I_a \otimes M_a$ is used as the query to localize the optimal correspondence region mask M^* in I_r . In the refinement stage, $I_r \otimes M^*$ is fed into DINOv2 (Oquab et al., 2023) encoder to extract expressive visual features, guiding the local generation process to eliminate the artifacts while ensuring identity preservation.

Our design is motivated by two key observations:

- Refine by localization: As summarized in (Zhang et al., 2023b), generative artifacts occurs more frequently around tiny object details such as logos, texts and other complex textures. However, these areas have higher fidelity when such details are prominent in the image. Based on this observation, we assume that the fidelity can be improved by performing a local generation guided by a local region from the reference.
- Align via cross-attention: As demonstrated in Hertz et al. (2022), the appearance of the generated image depends on the interaction between the pixels to the text embedding, which occurs in cross attention layers. Similarly, when replacing the text embedding with image embedding, we assume that spatial correspondence exists between the generated image and the image embedding.

Based on the above observations, we review cross-attention and prove that the spatial correspondence exists in Sec. 3.2; the algorithm to align $I_a \otimes M_a$ to the corresponding local region in I_r is explained in Sec. 3.3. Sec. 3.4 describes the two training modes. Sec. 3.5 describes the inference.

3.1 DIFFUSION MODEL

We leverage the architecture of AnyDoor (Chen et al., 2023) and IMPRINT (Song et al., 2024) as the backbone of our refinement network. It is based on the Stable Diffusion (Rombach et al., 2022) model, which contains three major components: the variational autoencoder (VAE) to code images into latent embeddings z , the U-Net backbone \mathcal{R} parameterized by θ for sequentially denoising diffusion steps on z by Gaussian noise ϵ , and a text encoder for guidance injection. We replace the text encoder by a vision encoder ϕ based on a pretrained DINOv2 (Oquab et al., 2023) to enable visual prompt guidance by a reference image $I_r \in \mathbb{R}^{H \times W \times 3}$ of a subject. In particular, the conditional embedding $\phi(I_r)$ will be utilized for optimization of loss functions on artifact refinement:

$$\mathcal{L}_{artifact} = \mathbb{E}_{z, I_r, \epsilon \sim \mathcal{N}(0, I), t} \left[\|\epsilon - \mathcal{R}_{\theta}(z_t, t, \phi(I_r))\|_2^2 \right] \quad (2)$$

where z_t is the latent embedding at time step t . \mathcal{R} is trained to iteratively denoise z_T to z_0 .

3.2 SPATIAL CORRESPONDENCE IN ENCODER-BASED CUSTOMIZATION MODELS

Our vision encoder ϕ based on DINOv2 is employed to extract the image embedding from the reference object, which is then fed to the cross attention layers of the U-Net backbone. Its ViT backbone divides the input image into 16×16 square patches, thus the encoded $\phi(I_r)$ is a sequence of 256 tokens and can be mapped back to 2D space with original spatial information as followed:

$$\mathbf{E} = \phi(I_r); \mathbf{E} \in \mathbb{R}^{256 \times d^{\phi}} \quad (3)$$

In each attention layer, $\phi(I_r)$ is projected to the key $\mathbf{k} = \psi_k(\mathbf{E})$ and the value $\mathbf{v} = \psi_v(\mathbf{E})$ by the linear projections ψ_k and ψ_v . Meanwhile, the noisy image encoded by VAE to latent embedding z_t is projected to the query $\mathbf{q} = \psi_q(z_t)$. Specifically, $z_t \in \mathbb{R}^{d \times c}$, where $d \in \{64, 32, 16, 8\}$ is the resolution of the extracted image features at different depth of layers, and c is the number of channels. z_t also contains spatial information. Altogether, the cross attention map \mathbf{A} is calculated as followed:

$$\mathbf{A} = \text{softmax}(\mathbf{q}\mathbf{k}^T); \mathbf{A} \in \mathbb{R}^{(d \times d) \times 256} \quad (4)$$

Intuitively, \mathbf{A} measures the similarity between \mathbf{q} and \mathbf{k} , and $\mathbf{A}_{[x, y, k]}$ stores the amount of information flow from the k th reference token to the latent pixel at (x, y) (Xiao et al., 2023). Therefore, through cross attention, \mathbf{A} effectively encodes the interaction between the noisy image and the reference embedding connected by spatial correlations.

3.3 THE ALIGNMENT ALGORITHM

Although the cross attention map \mathbf{A} encodes the spatial correlations between I_a and I_r , two challenges remain in identifying \mathbf{M}^* : (1) given \mathbf{A} , accurately locating the region in the reference image that corresponds to the free-form artifacts $I_a \otimes M_a$; (2) finding the optimal correspondence map \mathbf{M}^* from the numerous maps $\mathbf{M}^{t, l}$ of all possible combinations of diffusion timesteps t and transformer

layers l . Aiming at these two challenges, we present our **cross-attention alignment** algorithm, shown as pseudo code in Algorithm 1, and visualized in the top part of Fig. 5.

Optimal Cross-Attention Alignment

Since z_t is obtained by encoding a partially noisy version of I_a (see Sec. 3.4), each pixel $I_a[i, j]$ can be mapped to its spatial correspondence in z_t . Given that \mathbf{A} encodes the correlation between the noisy image z_t and the reference tokens \mathbf{E} (discussed in Sec. 3.2), it can be concluded that any pixel $I_a[i, j]$ can find its match in \mathbf{E} via \mathbf{A} .

For the correspondence map of I_r at diffusion timestep t and transformer layer l , we accomplish this by aggregating all pixels belonging to the artifacts:

$$\mathbf{M}^{t,l} = \sum_{i,j} (M_a \circ \mathbf{A}[i, j, :]) \quad (5)$$

where the Hadamard product is calculated between the artifacts mask and the cross-attention map. Intuitively, the 2D correspondence map $\mathbf{M}^{t,l}$ measures the similarity between all reference tokens and the artifacts pixels. To obtain the optimal \mathbf{M}^* , some post-processing needs to be applied on $\mathbf{M}^{t,l}$. Refer to Sec. A.4 for more details.

A grid search over all possible t, l values is performed on our proposed benchmark (see Sec. 4.1) and evaluated using mIoU. The results are shown in Fig. 4, demonstrating that the optimum combination is $t = 24$ and $l = 9$. However, during test time, we choose $t = 0, l = 9$ to accelerate the inference. Detailed comparisons can be found in Sec. 4.4.

3.4 TRAINING

For training, we implement two modes sharing weights of the same model, where the only difference lies in the inputs. In both modes, we train the U-Net, and the MLP connecting DINOv2 and U-Net.

Alignment Mode

To maximize the spatial correlations contained in the cross-attention maps, we design a fully self-supervised training scheme. The idea behind the construction of training pairs is: *Use a complete reference object to guide object completion, forcing the model to learn to identify the corresponding local region from the reference.*

We use Pixabay (Song et al., 2023) with panoptic segmentation labels as the training dataset. Following the aforementioned idea, given a Pixabay image I_o and an object mask M_o , we start by applying a random mask generator \mathcal{G} to sample a free-form artifacts mask $M_a = \mathcal{G}(M_o)$ within M_o . We then design color perturbation \mathcal{S} and affine transformations \mathcal{T} on $I_o \otimes M_o$ to simulate the lighting and view changes in the real world: $I_r = \mathcal{S}(\mathcal{T}(I_o \otimes M_o))$. In this mode, the artifacts image $I_a = I_o \times (1 - M_o)$ and the perturbed reference I_r are used as the inputs, and I_o is the target.

Refinement Mode

In this mode, it is assumed that the local region corresponding to the artifacts is already given from the original reference, which is used as I_r to guide the inpainting of the incomplete object.

Our training data consists of Pixabay and MVOBj, a manually annotated dataset where an object appears in multiple images with different contexts and views. MVOBj is added since our perturbations \mathcal{S}, \mathcal{T} are not sufficient to simulate non-rigid or 3D pose changes. 1) When dealing with a Pixabay image, we obtain the partial reference using the artifacts mask: $I_r = \mathcal{S}(\mathcal{T}(I_o \otimes M_a))$; 2) when processing a pair of MVOBj images $(I_{o1}, I_{o2}, M_{o1}, M_{o2})$, $I_{o1} \otimes \text{erode}(M_{o1})$ is used as the reference, and $I_{o2} \otimes 1 - (\text{erode}(M_{o2}))$ is the input artifacts image I_a , where the mask is eroded.

We then adopt the *zoom-in inpainting strategy* from Zhang et al. (2023b), cropping around I_a and perform inpainting on the zoom-in patch.

3.5 INFERENCE

Inference is performed in two stages, corresponding to the above two modes. In the alignment stage, given I_a, M_a, I_r , our fine-tuned model \mathcal{R} follows Alg. 1 and produces the correspondence map \mathbf{M}^* . Note that the grid search is skipped and \mathcal{R} only proceeds one timestep, directly producing the

Table 1: **Quantitative Comparison** with the baseline models on *GenArtifactBench*. PbE (Paint-by-Example) and OS (ObjectStitch) are finetuned on our training set; the local regions (instead of the complete reference) are provided to PbE, OS and AnyDoor. Our method outperforms the other baselines in fidelity. Since CLIP-T only captures high-level semantics, it cannot accurately measure the detail preservation. We show additional comparisons in Tab. 2 and Fig. 6.

Categories	Methods	CLIP-T \uparrow	CLIP-I \uparrow	DINO-I \uparrow
Reference-guided inpainting	Paint-by-Example*	23.5938	80.7500	58.7625
	ObjectStitch*	24.4844	83.9375	<u>72.6152</u>
	AnyDoor	25.0625	83.4375	71.3398
Text-guided inpainting	PAL	25.8906	81.5000	53.8117
Appearance transfer	Cross-Image Attention	23.2500	80.2500	56.7892
	MimicBrush	25.0156	<u>85.0625</u>	67.6194
	Ours	<u>25.4063</u>	86.6250	75.3135

optimal correspondence map M^* at timestep 0 and layer 9. The local region that corresponds to the artifacts can be extracted from the reference as $I_r \otimes M^*$.

In the refinement stage, $I_r \otimes M^*$ is provided as the reference through DINOv2, guiding the refinement of I_a via inpainting the artifacts region.

4 EXPERIMENT

4.1 EVALUATION BENCHMARK

Dataset. To provide insight on the appearance of generative artifacts and an effective evaluation of our artifacts refinement approach, we present **GenArtifactBench**, the first benchmark for reference-guided artifacts refinement (refer to the Appendix for examples), featuring:

- We generate images using four popular models: DreamBooth (Ruiz et al., 2023a), Zero123++ (Shi et al., 2023b), AnyDoor (Chen et al., 2023) and IDM-VTON (Choi et al., 2024), covering real-world applications of T2I customization, view synthesis, compositing and virtual try-on. Diverse artifacts are shown in these images.
- We collect 146 generated images with notable artifacts, paired with 146 reference images of more than 40 objects (from DreamBooth and Pixabay) and 27 garments (from Choi et al. (2021)).
- Human annotation of the artifacts, and the corresponding regions from the reference images.

Metrics. To measure the semantics and identity preservation of refined object, we utilize CLIP-Image Score (Radford et al., 2021) and DINO Score (Oquab et al., 2023) to compute the similarity between the refined region of the generated image and its corresponding region from the reference. When calculating CLIP-Text Score, BLIP2 (Li et al., 2023) is used to generate captions. Since a measurement of the overall quality is absent, we further conduct a user study.

Parameters. $t = 0$ and $l = 9$ are used in all the comparisons below.

4.2 QUANTITATIVE COMPARISONS

To demonstrate the effectiveness of our model, we compare our model with 6 baseline models (PbE or Paint-by-Example (Yang et al., 2023), OS or ObjectStitch (Song et al., 2023), AnyDoor (Chen et al., 2023), PAL (Zhang et al., 2023b), Cross-Image Attention (Alaluf et al., 2024) and MimicBrush (Chen et al., 2024), which is a *concurrent* work) on *GenArtifactBench* using the aforementioned metrics. For fair comparison, PbE and OS are fine-tuned on our training dataset.

Quantitative comparisons are shown in Tab. 1, where the baselines are categorized into three classes. Note that we provide the accurate reference regions for PbE, OS and AnyDoor, greatly reducing the difficulty for these models. In terms of semantics preservation measured by CLIP-T, PAL shows a slight advantage over our model; however, as illustrated in Fig.6, it fails to gain fine-grained control over the details in local editing. This is because PAL is built on SDXL (Podell et al., 2023), which



Figure 6: **Qualitative comparisons.** Zoom in to view details. Note that the accurate reference regions corresponding to the artifacts (not the complete reference) are provided to PbE, OS and AnyDoor. In the second row of the references, we overlay the correspondence maps on them. Compared with the baselines, our model not only preserves identity (most similar to the second row), but also generate smooth and natural results where artifacts are significantly reduced.

is only performing inpainting following a high-level text description. Our model outperforms all baseline models in details and appearance preservation. Owing to our correspondence matching strategy, irrelevant feature is removed and consequently the identity is significantly improved.

To take human perception into account as well as adding quality metrics, we conduct a user study on Amazon Mechanical Turk. We design two questions to assess identity preservation and generation realism, respectively. In each question, side-by-side comparisons are presented to the user: our result alongside one selected from a baseline. It is important to note that the reference images remain hidden from the user when assessing quality. Each question has 240 comparisons, and 720 votes are collected from more than 150 workers. The user preference is reported in Tab. 2. The preference rate demonstrates the superiority of our model over all baselines in both fidelity and realism.

Table 2: **User study.** Results are user preference win rate (%). Two questions are designed to measure identity preserving and realism; in each question the user is presented side-by-side results of our model and a random baseline. For fairness, PbE and OS are fine-tuned on our training dataset.

Identity \uparrow				Realism \uparrow			
Ours	70.83	Paint-by-Example*	29.17	Ours	71.67	Paint-by-Example*	28.33
Ours	55.83	ObjectStitch*	44.17	Ours	56.67	ObjectStitch*	43.33
Ours	57.50	AnyDoor	42.50	Ours	60.00	AnyDoor	40.00
Ours	74.17	Cross-Image Attention	25.83	Ours	83.33	Cross-Image Attention	16.67
Ours	61.67	PAL	38.33	Ours	71.67	PAL	28.33
Ours	60.00	MimicBrush	40.00	Ours	59.17	MimicBrush	40.83

4.3 QUALITATIVE RESULTS

Qualitative comparisons with the baseline models are shown in Fig. 6. The correspondence maps obtained by our model are overlaid on the reference image, highlighting the local regions that match the artifacts. When testing on PbE, OS and AnyDoor, these local regions (instead of the complete reference objects) are directly provided as input. In particular, PbE, OS and PAL struggle in preserving the finer details from the reference. This is especially the case for complex patterns since they only have high-level semantic control over the generation. AnyDoor can capture identity but fails to generate smooth transition areas. MimicBrush, a concurrent work, is designed for reference-guided local editing which shows superiorities over the other baselines; however, our model outperforms MimicBrush in both realism and fidelity.

4.4 ABLATION STUDY

Diffusion timestep and transformer layer. To evaluate the accuracy of the correspondence maps $M_{t,l}$, we ablate on all timesteps and layers $t \in \{0, 1, \dots, 49\}; l \in \{0, 1, \dots, 15\}$, and compute the mIoU over all images from *GenArtifactBench*, which is shown in Fig. 5. We also show a 2D mIoU figure on all combinations of t and l in the Appendix (Fig. 7), visualizing $\Gamma \in \mathbb{R}^{T \times L}$. To balance between efficiency and accuracy, we choose $t = 0, l = 9$.

Comparisons with keypoint matching. We compare our alignment algorithm to keypoint matching performance by two correspondence matching methods: DIFT (Tang et al., 2023) and DHF (Luo et al., 2023a). Visual results are in Fig. 2. While baselines struggle with repeating or irregular patterns, our alignment algorithm is more robust, with only a single query to locate the target region. Furthermore, the alignment and refinement stages are integrated into a unified model.

Ablation on model design. To demonstrate the effectiveness of our architecture design, we compare our full model with two settings (Tab. 3). 1) the model is only trained in the alignment mode, where a complete object is used as the reference. When the irrelevant patterns have been removed from the reference, identity preservation is significantly improved; 2) DINOv2 encoder is replaced by CLIP. The comparison proves that CLIP fails to encode low-level details, thus losing identity.

5 LIMITATIONS, CONCLUSION AND FUTURE WORK

We have shown a novel approach to artifact refinement via region alignment and reference-guided generation. Our approach makes use of a high-quality reference image to provide a predictable and controllable refinement output, that also preserves identity and transfers the details from the reference image to the input image containing artifacts. Our method has been compared to several baseline methods and has shown consistently superior performance. As limitations, first, our method does not always work well when there is a large disparity between the objects in the original input image and in the reference. Second, the accuracy of our alignment method is limited by the number of vision tokens, where only 16×16 patches are used to represent an image. As future work, we would like to extend our method to automate artifact detection and to incorporate the use of multiple reference images and text-descriptions so as to obtain blended outputs.

Table 3: **Ablation Study** on two model designs. 1) using a model which is only trained in the alignment mode to perform single stage artifacts refinement; 2) DINOv2 is replaced by CLIP encoder.

	CLIP-T \uparrow	CLIP-I \uparrow	DINO \uparrow
Single-stage	24.4375	84.5000	71.7609
CLIP-encoder	24.3750	84.3750	70.7714
Full	25.4063	86.6250	75.3135

REFERENCES

- Kfir Aberman, Jing Liao, Mingyi Shi, Dani Lischinski, Baoquan Chen, and Daniel Cohen-Or. Neural best-buddies: Sparse cross-domain correspondence. *ACM Transactions on Graphics (TOG)*, 37(4):1–14, 2018.
- Yuval Alaluf, Daniel Garibi, Or Patashnik, Hadar Averbuch-Elor, and Daniel Cohen-Or. Cross-image attention for zero-shot appearance transfer. In *ACM SIGGRAPH 2024 Conference Papers*, pp. 1–12, 2024.
- Omri Avrahami, Dani Lischinski, and Ohad Fried. Blended diffusion for text-driven editing of natural images. In *Proceedings of the IEEE/CVF Conference on Computer Vision and Pattern Recognition*, pp. 18208–18218, 2022.
- Herbert Bay, Tinne Tuytelaars, and Luc Van Gool. Surf: Speeded up robust features. In *Computer Vision—ECCV 2006: 9th European Conference on Computer Vision, Graz, Austria, May 7-13, 2006. Proceedings, Part I 9*, pp. 404–417. Springer, 2006.
- Bin Cao, Jianhao Yuan, Yexin Liu, Jian Li, Shuyang Sun, Jing Liu, and Bo Zhao. Synartifact: Classifying and alleviating artifacts in synthetic images via vision-language model. *arXiv preprint arXiv:2402.18068*, 2024.
- Xi Chen, Lianghua Huang, Yu Liu, Yujun Shen, Deli Zhao, and Hengshuang Zhao. Anydoor: Zero-shot object-level image customization. *arXiv preprint arXiv:2307.09481*, 2023.
- Xi Chen, Yutong Feng, Mengting Chen, Yiyang Wang, Shilong Zhang, Yu Liu, Yujun Shen, and Hengshuang Zhao. Zero-shot image editing with reference imitation. *arXiv preprint arXiv:2406.07547*, 2024.
- Seunghwan Choi, Sunghyun Park, Minsoo Lee, and Jaegul Choo. Viton-hd: High-resolution virtual try-on via misalignment-aware normalization. In *Proc. of the IEEE conference on computer vision and pattern recognition (CVPR)*, 2021.
- Yisol Choi, Sangkyung Kwak, Kyungmin Lee, Hyungwon Choi, and Jinwoo Shin. Improving diffusion models for virtual try-on. *arXiv preprint arXiv:2403.05139*, 2024.
- Timothée Darcet, Maxime Oquab, Julien Mairal, and Piotr Bojanowski. Vision transformers need registers. *arXiv preprint arXiv:2309.16588*, 2023.
- Rinon Gal, Yuval Alaluf, Yuval Atzmon, Or Patashnik, Amit H. Bermano, Gal Chechik, and Daniel Cohen-Or. An image is worth one word: Personalizing text-to-image generation using textual inversion, 2022. URL <https://arxiv.org/abs/2208.01618>.
- Sooyeon Go, Kyungmook Choi, Minjung Shin, and Youngjung Uh. Eye-for-an-eye: Appearance transfer with semantic correspondence in diffusion models. *arXiv preprint arXiv:2406.07008*, 2024.
- Jing Gu, Yilin Wang, Nanxuan Zhao, Tsu-Jui Fu, Wei Xiong, Qing Liu, Zhifei Zhang, He Zhang, Jianming Zhang, HyunJoon Jung, et al. Photoswap: Personalized subject swapping in images. *arXiv preprint arXiv:2305.18286*, 2023.
- Jing Gu, Yilin Wang, Nanxuan Zhao, Wei Xiong, Qing Liu, Zhifei Zhang, He Zhang, Jianming Zhang, HyunJoon Jung, and Xin Eric Wang. Swapanything: Enabling arbitrary object swapping in personalized visual editing. *arXiv preprint arXiv:2404.05717*, 2024.
- Eric Hedlin, Gopal Sharma, Shweta Mahajan, Hossam Isack, Abhishek Kar, Andrea Tagliasacchi, and Kwang Moo Yi. Unsupervised semantic correspondence using stable diffusion, 2023.
- Amir Hertz, Ron Mokady, Jay Tenenbaum, Kfir Aberman, Yael Pritch, and Daniel Cohen-Or. Prompt-to-prompt image editing with cross attention control. *arXiv preprint arXiv:2208.01626*, 2022.
- Jonathan Ho and Tim Salimans. Classifier-free diffusion guidance, 2022.

- Jonathan Ho, Ajay Jain, and Pieter Abbeel. Denoising diffusion probabilistic models. *Advances in Neural Information Processing Systems*, 33:6840–6851, 2020.
- Yuming Jiang, Kelvin CK Chan, Xintao Wang, Chen Change Loy, and Ziwei Liu. Reference-based image and video super-resolution via c2-matching. *IEEE Transactions on Pattern Analysis and Machine Intelligence*, 45(7):8874–8887, 2022.
- Bahjat Kawar, Shiran Zada, Oran Lang, Omer Tov, Huiwen Chang, Tali Dekel, Inbar Mosseri, and Michal Irani. Imagic: Text-based real image editing with diffusion models. In *Proceedings of the IEEE/CVF Conference on Computer Vision and Pattern Recognition*, pp. 6007–6017, 2023.
- Nupur Kumari, Bingliang Zhang, Richard Zhang, Eli Shechtman, and Jun-Yan Zhu. Multi-concept customization of text-to-image diffusion. In *Proceedings of the IEEE/CVF Conference on Computer Vision and Pattern Recognition*, pp. 1931–1941, 2023.
- Junnan Li, Dongxu Li, Silvio Savarese, and Steven Hoi. Blip-2: Bootstrapping language-image pre-training with frozen image encoders and large language models. *arXiv preprint arXiv:2301.12597*, 2023.
- Nannan Li, Qing Liu, Krishna Kumar Singh, Yilin Wang, Jianming Zhang, Bryan A Plummer, and Zhe Lin. Unihuman: A unified model for editing human images in the wild. In *Proceedings of the IEEE/CVF Conference on Computer Vision and Pattern Recognition*, pp. 2039–2048, 2024.
- Minghua Liu, Ruoxi Shi, Linghao Chen, Zhuoyang Zhang, Chao Xu, Xinyue Wei, Hansheng Chen, Chong Zeng, Jiayuan Gu, and Hao Su. One-2-3-45++: Fast single image to 3d objects with consistent multi-view generation and 3d diffusion. In *Proceedings of the IEEE/CVF Conference on Computer Vision and Pattern Recognition*, pp. 10072–10083, 2024.
- Ruoshi Liu, Rundui Wu, Basile Van Hoorick, Pavel Tokmakov, Sergey Zakharov, and Carl Vondrick. Zero-1-to-3: Zero-shot one image to 3d object. In *Proceedings of the IEEE/CVF International Conference on Computer Vision*, pp. 9298–9309, 2023a.
- Zhiheng Liu, Ruili Feng, Kai Zhu, Yifei Zhang, Kecheng Zheng, Yu Liu, Deli Zhao, Jingren Zhou, and Yang Cao. Cones: Concept neurons in diffusion models for customized generation. *arXiv preprint arXiv:2303.05125*, 2023b.
- David G Lowe. Distinctive image features from scale-invariant keypoints. *International journal of computer vision*, 60:91–110, 2004.
- Shilin Lu, Yanzhu Liu, and Adams Wai-Kin Kong. Tf-icon: Diffusion-based training-free cross-domain image composition. In *Proceedings of the IEEE/CVF International Conference on Computer Vision*, pp. 2294–2305, 2023.
- Grace Luo, Lisa Dunlap, Dong Huk Park, Aleksander Holynski, and Trevor Darrell. Diffusion hyperfeatures: Searching through time and space for semantic correspondence. In *Advances in Neural Information Processing Systems*, 2023a.
- Simian Luo, Yiqin Tan, Longbo Huang, Jian Li, and Hang Zhao. Latent consistency models: Synthesizing high-resolution images with few-step inference. *arXiv preprint arXiv:2310.04378*, 2023b.
- Chenlin Meng, Yutong He, Yang Song, Jiaming Song, Jiajun Wu, Jun-Yan Zhu, and Stefano Ermon. Sdedit: Guided image synthesis and editing with stochastic differential equations. *arXiv preprint arXiv:2108.01073*, 2021.
- Maxime Oquab, Timothée Darcet, Theo Moutakanni, Huy V. Vo, Marc Szafraniec, Vasil Khalidov, Pierre Fernandez, Daniel Haziza, Francisco Massa, Alaaeldin El-Nouby, Russell Howes, Po-Yao Huang, Hu Xu, Vasu Sharma, Shang-Wen Li, Wojciech Galuba, Mike Rabbat, Mido Assran, Nicolas Ballas, Gabriel Synnaeve, Ishan Misra, Herve Jegou, Julien Mairal, Patrick Labatut, Armand Joulin, and Piotr Bojanowski. Dinov2: Learning robust visual features without supervision, 2023.
- William Peebles and Saining Xie. Scalable diffusion models with transformers. In *Proceedings of the IEEE/CVF International Conference on Computer Vision*, pp. 4195–4205, 2023.

- Dustin Podell, Zion English, Kyle Lacey, Andreas Blattmann, Tim Dockhorn, Jonas Müller, Joe Penna, and Robin Rombach. Sdxl: Improving latent diffusion models for high-resolution image synthesis. *arXiv preprint arXiv:2307.01952*, 2023.
- Alec Radford, Jong Wook Kim, Chris Hallacy, Aditya Ramesh, Gabriel Goh, Sandhini Agarwal, Girish Sastry, Amanda Askell, Pamela Mishkin, Jack Clark, et al. Learning transferable visual models from natural language supervision. In *International Conference on Machine Learning*, pp. 8748–8763. PMLR, 2021.
- Ignacio Rocco, Mircea Cimpoi, Relja Arandjelović, Akihiko Torii, Tomas Pajdla, and Josef Sivic. Neighbourhood consensus networks. *Advances in neural information processing systems*, 31, 2018.
- Robin Rombach, Andreas Blattmann, Dominik Lorenz, Patrick Esser, and Björn Ommer. High-resolution image synthesis with latent diffusion models. In *Proceedings of the IEEE/CVF Conference on Computer Vision and Pattern Recognition*, pp. 10684–10695, 2022.
- Ethan Rublee, Vincent Rabaud, Kurt Konolige, and Gary Bradski. Orb: An efficient alternative to sift or surf. In *2011 International conference on computer vision*, pp. 2564–2571. Ieee, 2011.
- Nataniel Ruiz, Yuanzhen Li, Varun Jampani, Yael Pritch, Michael Rubinstein, and Kfir Aberman. Dreambooth: Fine tuning text-to-image diffusion models for subject-driven generation. In *Proceedings of the IEEE/CVF Conference on Computer Vision and Pattern Recognition*, pp. 22500–22510, 2023a.
- Nataniel Ruiz, Yuanzhen Li, Varun Jampani, Wei Wei, Tingbo Hou, Yael Pritch, Neal Wadhwa, Michael Rubinstein, and Kfir Aberman. Hyperdreambooth: Hypernetworks for fast personalization of text-to-image models. *arXiv preprint arXiv:2307.06949*, 2023b.
- Vishnu Sarukkai, Linden Li, Arden Ma, Christopher Ré, and Kayvon Fatahalian. Collage diffusion. In *Proceedings of the IEEE/CVF Winter Conference on Applications of Computer Vision*, pp. 4208–4217, 2024.
- Paul Hongsuck Seo, Jongmin Lee, Deunsol Jung, Bohyung Han, and Minsu Cho. Attentive semantic alignment with offset-aware correlation kernels. In *Proceedings of the European Conference on Computer Vision (ECCV)*, pp. 349–364, 2018.
- Jing Shi, Wei Xiong, Zhe Lin, and Hyun Joon Jung. Instantbooth: Personalized text-to-image generation without test-time finetuning. *arXiv preprint arXiv:2304.03411*, 2023a.
- Ruoxi Shi, Hansheng Chen, Zhuoyang Zhang, Minghua Liu, Chao Xu, Xinyue Wei, Linghao Chen, Chong Zeng, and Hao Su. Zero123++: a single image to consistent multi-view diffusion base model. *arXiv preprint arXiv:2310.15110*, 2023b.
- Karen Simonyan, Andrea Vedaldi, and Andrew Zisserman. Learning local feature descriptors using convex optimisation. *IEEE Transactions on Pattern Analysis and Machine Intelligence*, 36(8): 1573–1585, 2014.
- Jascha Sohl-Dickstein, Eric Weiss, Niru Maheswaranathan, and Surya Ganguli. Deep unsupervised learning using nonequilibrium thermodynamics. In *International Conference on Machine Learning*, pp. 2256–2265. PMLR, 2015.
- Yang Song and Stefano Ermon. Generative modeling by estimating gradients of the data distribution. *Advances in Neural Information Processing Systems*, 32, 2019.
- Yizhi Song, Zhifei Zhang, Zhe Lin, Scott Cohen, Brian Price, Jianming Zhang, Soo Ye Kim, and Daniel Aliaga. Objectstitch: Object compositing with diffusion model. In *Proceedings of the IEEE/CVF Conference on Computer Vision and Pattern Recognition*, pp. 18310–18319, 2023.
- Yizhi Song, Zhifei Zhang, Zhe Lin, Scott Cohen, Brian Price, Jianming Zhang, Soo Ye Kim, He Zhang, Wei Xiong, and Daniel Aliaga. Imprint: Generative object compositing by learning identity-preserving representation. In *Proceedings of the IEEE/CVF Conference on Computer Vision and Pattern Recognition*, pp. 8048–8058, 2024.

- Luming Tang, Menglin Jia, Qianqian Wang, Cheng Perng Phoo, and Bharath Hariharan. Emergent correspondence from image diffusion. In *Thirty-seventh Conference on Neural Information Processing Systems*, 2023. URL <https://openreview.net/forum?id=ypOiXjdfnU>.
- Luming Tang, Nataniel Ruiz, Qinghao Chu, Yuanzhen Li, Aleksander Holynski, David E Jacobs, Bharath Hariharan, Yael Pritch, Neal Wadhwa, Kfir Aberman, et al. Realfill: Reference-driven generation for authentic image completion. *ACM Transactions on Graphics (TOG)*, 43(4):1–12, 2024.
- Benzhi Wang, Jingkai Zhou, Jingqi Bai, Yang Yang, Weihua Chen, Fan Wang, and Zhen Lei. Realishuman: A two-stage approach for refining malformed human parts in generated images. *arXiv preprint arXiv:2409.03644*, 2024a.
- Yibin Wang, Weizhong Zhang, Jianwei Zheng, and Cheng Jin. Primecomposer: Faster progressively combined diffusion for image composition with attention steering. *arXiv preprint arXiv:2403.05053*, 2024b.
- Guangxuan Xiao, Tianwei Yin, William T Freeman, Frédo Durand, and Song Han. Fastcomposer: Tuning-free multi-subject image generation with localized attention. *arXiv preprint arXiv:2305.10431*, 2023.
- Binxin Yang, Shuyang Gu, Bo Zhang, Ting Zhang, Xuejin Chen, Xiaoyan Sun, Dong Chen, and Fang Wen. Paint by example: Exemplar-based image editing with diffusion models. In *Proceedings of the IEEE/CVF Conference on Computer Vision and Pattern Recognition*, pp. 18381–18391, 2023.
- Junyi Zhang, Charles Herrmann, Junhwa Hur, Luisa Polania Cabrera, Varun Jampani, Deqing Sun, and Ming-Hsuan Yang. A tale of two features: Stable diffusion complements dino for zero-shot semantic correspondence. 2023a.
- Lingzhi Zhang, Zhengjie Xu, Connelly Barnes, Yuqian Zhou, Qing Liu, He Zhang, Sohrab Amirghodsi, Zhe Lin, Eli Shechtman, and Jianbo Shi. Perceptual artifacts localization for image synthesis tasks. In *Proceedings of the IEEE/CVF International Conference on Computer Vision*, pp. 7579–7590, 2023b.
- Lvmin Zhang, Anyi Rao, and Maneesh Agrawala. Adding conditional control to text-to-image diffusion models, 2023c.
- Yuxuan Zhang, Yiren Song, Jiaming Liu, Rui Wang, Jinpeng Yu, Hao Tang, Huaxia Li, Xu Tang, Yao Hu, Han Pan, et al. Ssr-encoder: Encoding selective subject representation for subject-driven generation. In *Proceedings of the IEEE/CVF Conference on Computer Vision and Pattern Recognition*, pp. 8069–8078, 2024.
- Zhifei Zhang, Zhaowen Wang, Zhe Lin, and Hairong Qi. Image super-resolution by neural texture transfer. In *Proceedings of the IEEE/CVF conference on computer vision and pattern recognition*, pp. 7982–7991, 2019.
- Yuqian Zhou, Connelly Barnes, Eli Shechtman, and Sohrab Amirghodsi. Transfill: Reference-guided image inpainting by merging multiple color and spatial transformations. In *Proceedings of the IEEE/CVF conference on computer vision and pattern recognition*, pp. 2266–2276, 2021.

A APPENDIX

A.1 ABLATION STUDY ON TIMESTEP AND LAYER

Since Fig.5 in the main paper only shows the effect of either changing the timestep t or changing the layer l , we also show a 2D mIoU map on all possible combinations of t and l , visualizing $\Gamma \in \mathbb{R}^{T \times L}$ in Fig. 7. It can be concluded that the information of spatial correlation encoded in a layer is similar across all timesteps; and the information stored in different layers varies dramatically, where the most precise correlation is mirrored in layer 9.

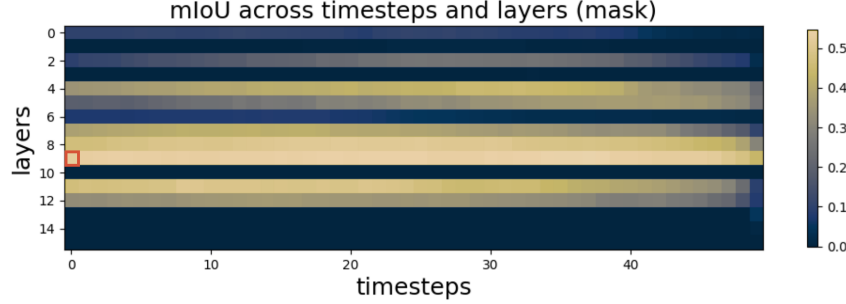


Figure 7: Grid-search results of all transformer layers and diffusion time steps. The 2D heatmap shows mIoU over all possible combinations of the parameters. The highlighted block is our chosen setting for running the inference.

A.2 ANALYSIS OF PERCEPTUAL ARTIFACTS

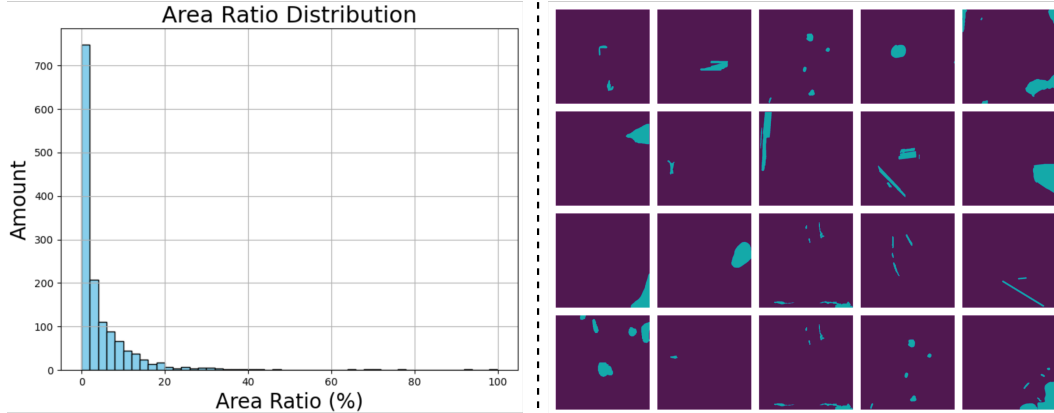


Figure 8: Statistics of PAL artifacts dataset (Zhang et al., 2023b). Left: Visualization of the distribution of the artifacts area ratio, calculated from 1405 annotated artifact images. The histogram demonstrates that generative artifacts are usually *tiny*; Right: Visualization of the artifact masks randomly selected. It demonstrates that most artifacts are tiny and *irregular-shaped*.

Since PAL released a large-scale dataset for artifacts detection containing generated images and segmentation labels, we perform a data analysis on a randomly chosen subset. In Fig. 8, the histogram on the left shows the distribution of the area ratio of artifacts; the figure on the right visualizes the artifact masks sampled from the dataset. The conclusions can be summarized as follows:

- Artifact regions are typically very small, with the artifact area covering less than 4% of the entire image in more than 50% of cases.
- Artifacts exhibit irregular shapes.

The design of our refinement model is motivated by these observations.

A.3 TRAINING DETAILS

Our training set consists of 1) Pixabay, a dataset of 116k images; 2) MVObj, a dataset of 51k paired images. We train the model with a batch size of 192 and drop the image embedding at a rate of 0.1. The learning rate of the MLP connecting DINOv2 and U-Net is 4×10^{-5} , and the U-Net has a learning rate of 1×10^{-5} . The model is trained for more than 45 epochs on 8 NVIDIA A100 GPUs.

A.4 POST-PROCESSING OF THE CORRESPONDENCE MAP

We apply some post-processing on the raw $M^{t,l}$ to obtain the optimal correspondence map M^* which is clean. As Darcet et al. (2023) pointed out, noise is often identified around the corners and boundaries in feature maps of ViT networks. Since such noise is also observed in our case, we utilize a noise filter to remove it via peak detection. After noise removal, there are only a few blobs left; and we simply adopt a clustering algorithm to locate the largest blob as the corresponding region.

A.5 USER STUDY

We show the two sections of our user study in Fig. 9 and Fig. 10, measuring realism and fidelity respectively. Note that the images shown in the figures here have been resized for display purposes (thus appearing smaller) and do not reflect their actual sizes used in the user study.

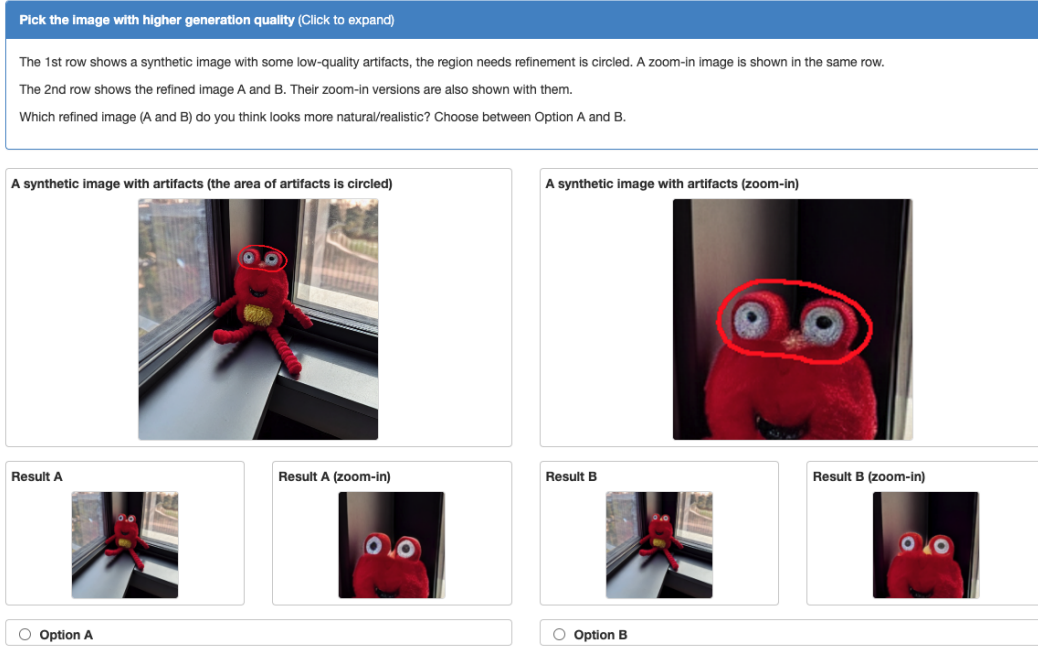


Figure 9: User interface of the user study evaluating the overall quality.

A.6 GENARTIFACTBENCH

The features of proposed benchmark, *GenArtifactBench*, are listed in Sec. 4.1. We collect 146 images groups for four tasks: Text-to-Image customization, novel view synthesis, object composition and virtual try-on; the synthetic images are generated by DreamBooth (Ruiz et al., 2023a), Zero123++ (Shi et al., 2023b), AnyDoor (Chen et al., 2023) and IDM-VTON Choi et al. (2024). Fig. 11 shows one example for each task.

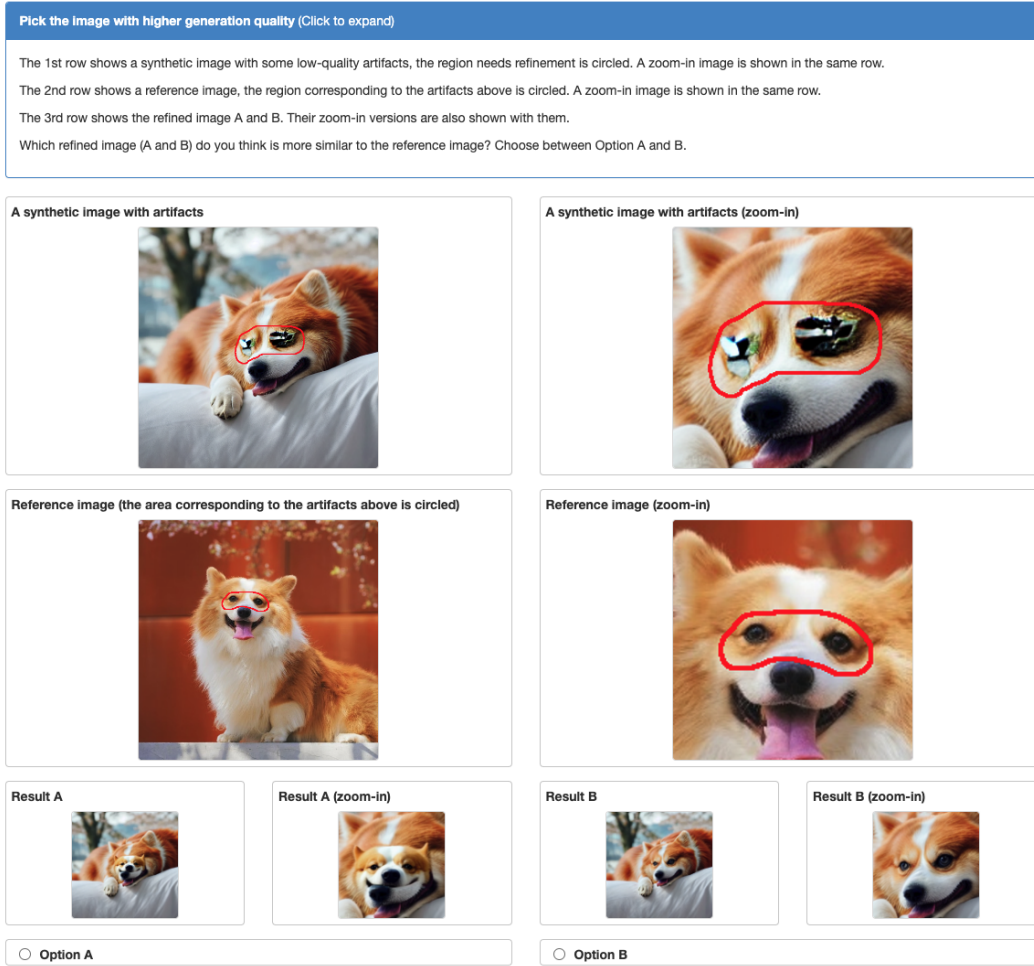


Figure 10: User interface of the user study evaluating identity preservation.

A.7 ADDITIONAL QUALITATIVE RESULTS

We include more qualitative results in Fig. 12.

A.8 EXAMPLES OF THE MVOBJ DATASET

As part of our training dataset, we have collected *MVObj*, an object-centric paired dataset. Examples are displayed in Fig. 13.

A.9 CORRESPONDENCE MATCHING USING ANYDOOR

When integrated with our cross-attention alignment algorithm, AnyDoor demonstrates the capability to perform semantic alignment. However, this ability is significantly limited in its original checkpoint, resulting in low alignment accuracy. We show a few examples in Fig. 14. In contrast, we propose a specialized training scheme (Sec. 3.4) to enhance the alignment accuracy of our model.

A.10 QUALITATIVE STUDY OF THE ROBUSTNESS

In real-world applications, the generated images exhibit significant diversity in structure and appearance, making it essential to evaluate the robustness of our model, especially in cases where artifact

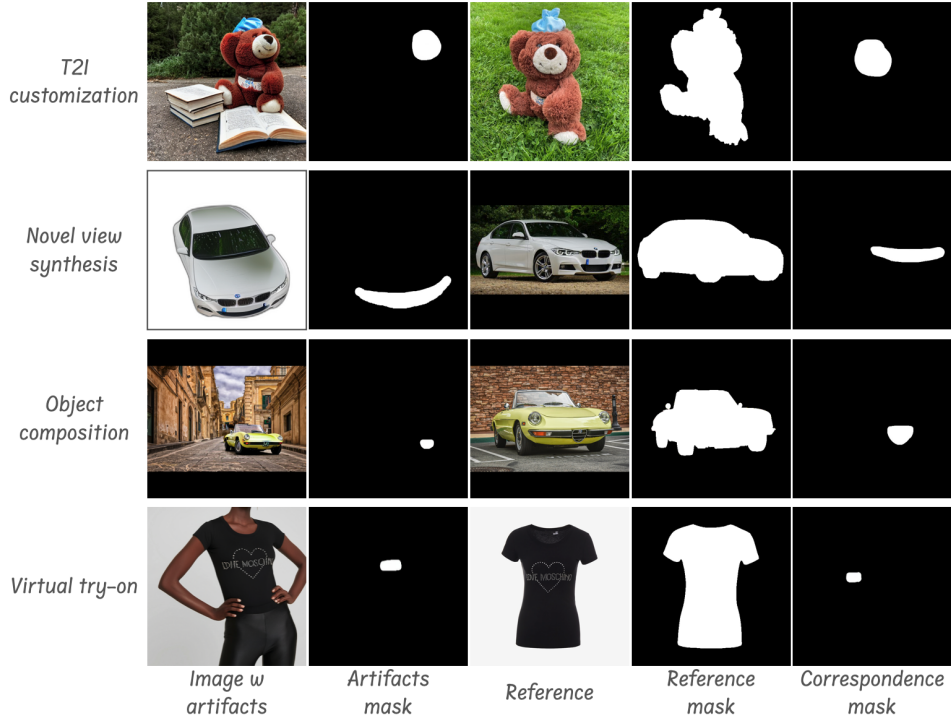
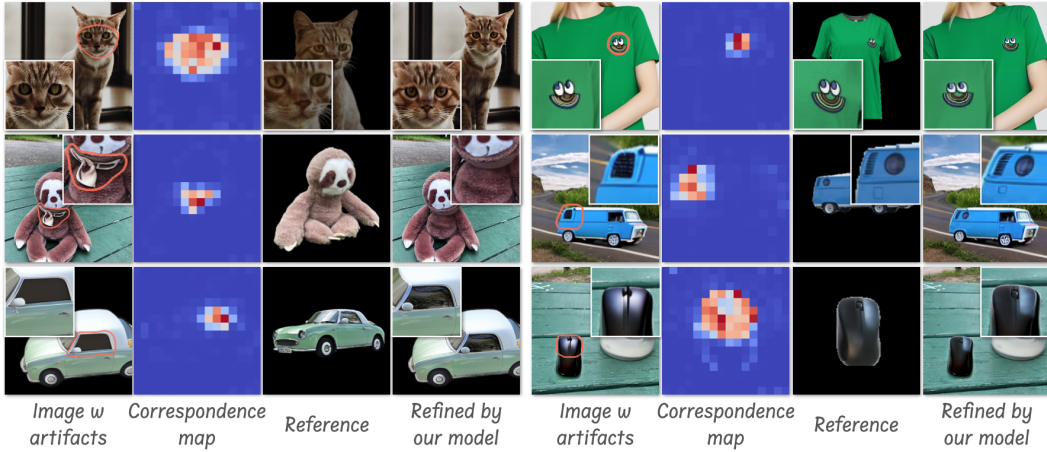
Figure 11: Example images of our proposed benchmark, *GenArtifactBench*.

Figure 12: More qualitative results.

regions and reference objects differ substantially in appearance. As shown in Fig. 15, we selected examples where the images with artifacts and the references have a substantial domain gap in content. We then applied our refinement model to locate the correspondences in the references. The results demonstrate the robustness of our model.

A.11 AN IMAGE DEGRADATION SIMULATION PIPELINE

As part of future work to enhance the generalization ability of our model to diverse artifacts, we propose an artifact simulation pipeline that introduces random artifacts into images (displayed in Fig. 16). This pipeline ensures that the artifacts are always generated within the object, and the original layout and background are always preserved. Fig. 17 displays several examples.



Figure 13: A few paired images of the training dataset MVOBJ.

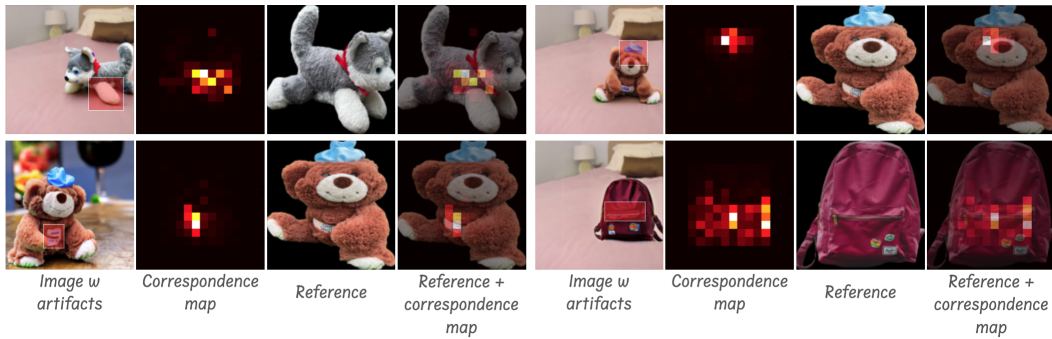


Figure 14: Correspondence matching using the original AnyDoor checkpoint. Given an image where the artifacts has been marked, we leverage the original AnyDoor checkpoint and apply our cross-attention alignment algorithm (Sec. 3.3) for local region matching. The corresponding region in the reference image is indicated by the correspondence map. As shown by the results, AnyDoor cannot accurately find the correspondence.

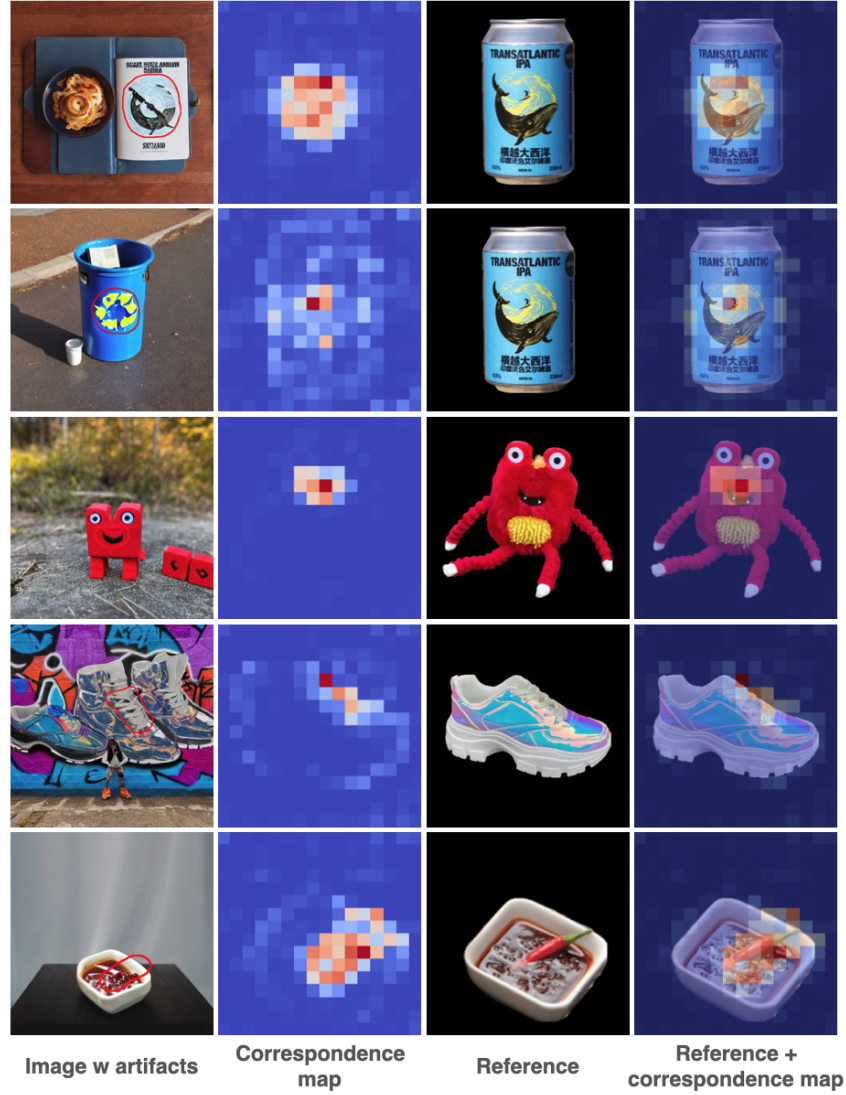


Figure 15: Qualitative analysis of the robustness of the input data. The first column shows the generated images, with artifacts highlighted by red circles. Given the generated images (first column) and the references (third column), our model generates the correspondence maps (second column). Even when the artifact regions and reference objects differ significantly in appearance (e.g., shape, texture, or color), our model is capable of achieving accurate alignment.

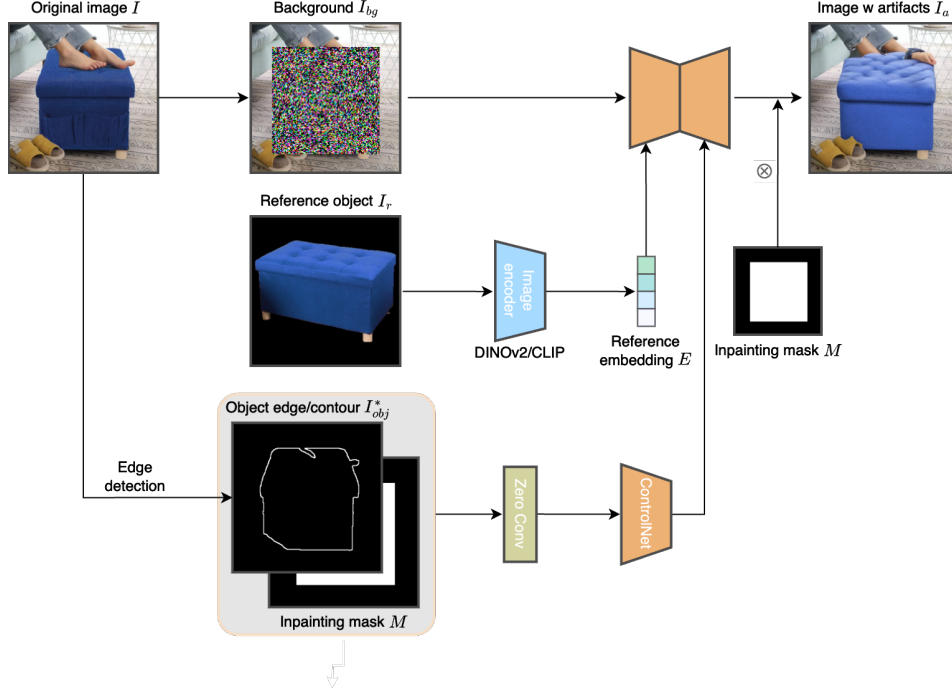


Figure 16: A pipeline to simulate generative artifacts. Given an image pair (I, I_r) (the pair should contain the same object; e.g., a pair from MVOBJ dataset), the proposed simulation system reconstructs image I using I_r as the reference guidance. To preserve the original layout and structure of I , we leverage a ControlNet (Zhang et al., 2023c) conditioned on the object edges of I . As a result, an image I_a is generated, where the object has perceptual artifacts of internal structure and texture.

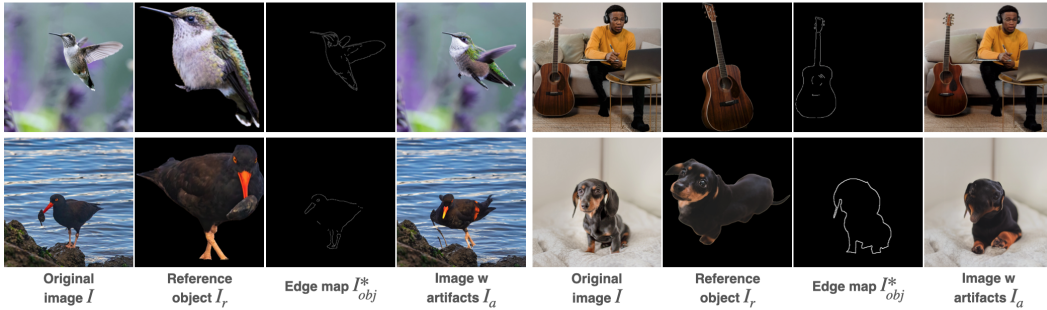


Figure 17: Generative artifacts produced by the degradation simulation pipeline in Fig. 16. Given a pair of images (I, I_r) , an edge map I_{obj}^* is predicted from I and fed to the ControlNet. In the simulation pipeline, both I_{obj}^* and I_r are provided as guidance to reconstruct I . The simulation system generates I_a , which contains artifacts within the object as well as preserving the original layout and background.